Inorganic Chemistry
Cite This: Inorg. Chem. 2019, 58, 4657−4664
Article
pubs.acs.org/IC

Enantiomeric Polyoxometalates Based on Malate Chirality-Inducing Tetra-Zr^{IV}−Substituted Keggin Dimeric Clusters

Yue-Lin Wang,[†] Jun-Wei Zhao,*[,‡] Zhong Zhang,[†] Jun-Jun Sun,[†] Xu-Yan Li,[†] Bai-Feng Yang,[†] and Guo-Yu Yang*[,†]

[†]MOE Key Laboratory of Cluster Science, School of Chemistry and Chemical Engineering, Beijing Institute of Technology, Beijing 102488, People's Republic of China

[‡]Henan Key Laboratory of Polyoxometalate Chemistry, College of Chemistry and Chemical Engineering, Henan University, Kaifeng, Henan 475004, People's Republic of China

Supporting Information

ABSTRACT: On the basis of the synergistic strategy of lacunary polyoxometalate structure-directing function and chiral ligand inducting role, two pairs of enantiomeric polyoxotungstates, $(NH_4)_4(TMA)_4[Zr_4(\mu_3\text{-}O)_2(L\text{-}/D\text{-}mal)_2(B\text{-}\alpha\text{-}HSiW_{10}O_{37})_2]$ (TMA = tetramethylammonium, mal = malate ($C_4H_5O_5$); L-mal for **1a**, D-mal for **1b**) and $(NH_4)_4(TMA)_4[Zr_4(\mu_3\text{-}O)_2(L\text{-}/D\text{-}mal)_2(B\text{-}\alpha\text{-}PW_{10}O_{37})_2]$ (L-mal for **2a**, D-mal for **2b**), and a mesomeric polyoxotungstate, $(NH_4)_3Na_2K_5[Zr_4(\mu_3\text{-}O)_2(L\text{-mal})(D\text{-mal})(B\text{-}\alpha\text{-}SiW_{10}O_{37})_2]$ (**3**), were hydrothermally synthesized. **1a**, **2a** and **1b**, **2b** respectively exhibit 1-D 2_1 right- and left-hand helical chains formed by hydrogen-bonding interactions, and **3** forms a 3-D (3,10)-connected framework by Na^+/K^+ ions with $\{4^{18}.6^{24}.8^3\}\{4^3\}_2$ topology. These homochiral compounds represent the first examples of enantiomerically pure Zr^{IV}-substituted Keggin POMs. In this system, $\{Zr_4(\mu_3\text{-}O)_2(L\text{-}/D\text{-}mal)_2\}$ clusters transfer chirality from D- or L-mal to Keggin polyoxotungstate dimeric clusters, which was demonstrated by structural comparison between the homochiral architecture and mesomer as well as circular dichroism spectra of enantiomers. UV−vis diffuse reflectance spectra reveal that **1**−**3** are potential semiconductor materials. In addition, **1** and **2** exhibit second harmonic generation response with their response intensities of 0.8 times that of KDP.

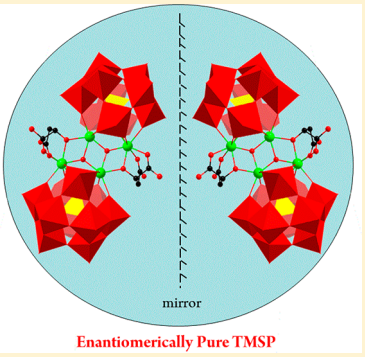

INTRODUCTION

Homochiral materials have remained the subjects of considerable focus not only because of their intriguing architectural diversity but also due to their potential applications in many different areas such as enantioselective separation and catalysis, nonlinear optics, and biology.[1−15] Polyoxometalates (POMs), as a large class of anionic metal−oxygen cluster species, have attracted extensive interest due to their flexible structures, enormous compositions, and special properties applicable to magnetism, catalysis, biology, medicine, and materials science.[16−32] The introduction of chirality into POMs can further endow them with special functions.[33−40] However, it is difficult to control the chirality of POMs because most chiral POMs are inclined to rapid racemization via rearrangements in solution as well as in the solid state.[41−43] As a result, creating chiral POM-based materials (PBMs) has become an interesting and challenging topic.

Generally, chiral PBMs can be divided into two categories: pure inorganic chiral PBMs and inorganic−organic hybrid chiral PBMs. In this context, great efforts have been devoted to exploring the formation of chiral PBMs and three different strategies have been proposed. First, the method of spontaneous symmetry breaking was used to synthesize PBMs crystallizing in a chiral space group. A few interesting findings from this approach have been reported by the groups of Knoth, Liu, and Yang.[44−46] Second, chiral PBMs were prepared through electrostatic interactions between polyoxoanions and chiral cations or carriers. For example, Wu et al. employed organic chiral cations to replace inorganic counterions of POMs, resulting in the formation of two chiral organic-cation-encapsulated PBMs in 2012.[47] More recently, Nlate and co-workers addressed a series of chiral optically active silica POM-based nanohelices through attaching achiral POM clusters onto chiral silica nanohelices by electrostatic coupling interactions.[48] The third strategy is based on covalent connecting of POM clusters with chiral units (organic ligands or metal−organic complexes) to construct chiral PBMs. For instance, Peng obtained two pairs of enantiopure hybrids containing covalently linked Lindqvist PBMs with C_2-symmetric binaphthyl units, showing moderate chiroptical behavior in solution.[49] Carraro and co-workers made chiral PBMs by covalent grafting of chiral phosphoryl groups onto the divacant $[\gamma\text{-}GeW_{10}O_{36}]^{8-}$ cluster surface.[50] Furthermore, the Wang and Su group communicated two chiral PBMs constructed from $[BW_{12}O_{40}]^{5-}$ polyoxoanions and copper−amino acid complexes.[2] In these cases, the chirality of organic

Received: January 27, 2019
Published: March 18, 2019

DOI: 10.1021/acs.inorgchem.9b00258
Inorg. Chem. 2019, 58, 4657−4664

Table 1. Crystallographic Data and Structural Refinements for 1−3

	1a	1b	2a	2b	3
formula	$C_{24}H_{114}N_8O_{105}Si_2W_{20}Zr_4$	$C_{24}H_{124}N_8O_{110}Si_2W_{20}Zr_4$	$C_{24}H_{102}N_8O_{100}P_2W_{20}Zr_4$	$C_{24}H_{96}N_8O_{97}P_2W_{20}Zr_4$	$C_8H_{78}N_3O_{114}K_5Na_2Si_2W_{20}Zr_4$
M_r	6293.29	6383.36	6206.95	6152.9	6380.27
cryst syst	orthorhombic	orthorhombic	orthorhombic	orthorhombic	monoclinic
space group	$P2_12_12_1$	$P2_12_12_1$	$P2_12_12_1$	$P2_12_12_1$	$C2/c$
a (Å)	20.2216(5)	20.1837(13)	20.1837(6)	20.2427(6)	36.9052(10)
b (Å)	25.0383(8)	24.8743(19)	24.9066(10)	24.8628(7)	12.2799(5)
c (Å)	25.9643(8)	25.834(2)	25.9941(8)	26.0152(6)	24.5473(12)
α (deg)	90	90	90	90	90
β (deg)	90	90	90	90	94.233(3)
γ (deg)	90	90	90	90	90
V (Å^3)	13146.1(7)	12970.1(16)	13067.4(8)	13093.2(6)	11094.3(8)
Z, D_c (g cm^{-3})	4, 3.180	4, 3.269	4, 3.155	4, 3.121	4, 3.820
F(000)	11288	11488	11088	10968	11376
T (K)	293(2)	293(2)	293(2)	293(2)	293(2)
μ (mm^{-1})	17.843	18.090	17.951	17.913	21.340
no. of rflns coll	51287	49527	46519	52140	29145
no. of unique rflns	22105	22264	21802	22926	9754
no. of params	1234	1243	1234	1243	646
GOF on F^2	1.013	1.001	1.023	1.034	1.037
final R indices ($I > 2\sigma(I)$)	R1 = 0.0513	R1 = 0.0445	R1 = 0.0460	R1 = 0.0489	R1 = 0.0592
	wR2 = 0.1173	wR2 = 0.0682	wR2 = 0.0778	wR2 = 0.1214	wR2 = 0.1510
R indices (all data)[a]	R1 = 0.0697	R1 = 0.0692	R1 = 0.0685	R1 = 0.0662	R1 = 0.0788
	wR2 = 0.1274	wR2 = 0.0762	wR2 = 0.0841	wR2 = 0.1319	wR2 = 0.1645
peak/hole (e/Å^{-3})[a]	2.280/−2.309	1.481/−1.612	1.783/−1.735	2.519/−1.750	4.846/−3.635
Flack param	−0.008(7)	−0.021(8)	−0.029(9)	0.001(5)	

[a] $R_1 = \sum||F_0|-|F_c||/\sum|F_0|$. $wR_2 = [\sum w(F^2_0 - F^2_c)^2/\sum w(F^2_0)^2]^{1/2}$

DOI: 10.1021/acs.inorgchem.9b00258
Inorg. Chem. 2019, 58, 4657−4664

moieties is transferred to the POM frameworks. Evidently, covalent functionalization of POM clusters with chiral units is an efficient and promising approach to make chiral PBMs and allows their properties to be tuned.[34] However, chiral ligand modified transition-metal-substituted POMs (TMSPs) remain extremely less explored. To the best of our knowledge, there are few examples of organic ligand chirality-induced TMSPs. For example, Hill et al. reported the pair of chiral tartrate-functionalized Zr^{IV}-substituted Dawson POMs $[(CH_3)_2NH_2]_{15}\{[\alpha\text{-}P_2W_{15}O_{55}(H_2O)]Zr_3(\mu_3\text{-}O)(H_2O)(\text{L-/D-tartH})[\alpha\text{-}P_2W_{16}O_{59}]\}\cdot 18H_2O$ in 2005,[42] and subsequently, by increasing the number of chiral ligands, a other Dawson-based enantiomers were isolated.[43] Mizuno et al. documented two chiral TMSPs $TBA_4[\gamma\text{-}SiTi_2W_{10}O_{36}(\mu\text{-}OH)_2(R\text{-}/S\text{-}BINOLate)]$ by introducing stereoisomeric naphthol groups into Ti_2-substituted POMs in 2015.[51] Hence, chiral-ligand-functionalized TMSPs have aroused our intense attraction.

Here, we chose trilacunary Keggin $\{A\text{-}\alpha\text{-}XW_9O_{34}\}$ ($X = P^V$, Si^{IV}) precursors to react with $ZrOCl_2$ and D-/L-mal on the basis of the following considerations. (1) The lacunary sites of $\{A\text{-}\alpha\text{-}XW_9O_{34}\}$ fragments can act as structure-directing agents and induce in situ aggregation of transition-metal (TM) ions to form larger TM clusters in the vacancy of POM fragments under hydrothermal conditions, which has been adequately demonstrated by our previous work.[52−55] Moreover, trilacunary Keggin $\{A\text{-}\alpha\text{-}XW_9O_{34}\}$ can be easily prepared as starting materials with high yield and are stable in an atmospheric environment. In addition, trilacunary Keggin $\{A\text{-}\alpha\text{-}XW_9O_{34}\}$ derivatives have several isostructures such as $\{B\text{-}\alpha\text{-}XW_9O_{34}\}$, $\{A\text{-}\beta\text{-}XW_9O_{34}\}$, and $\{B\text{-}\beta\text{-}XW_9O_{34}\}$.[56] (2) Commonly, the Zr^{IV} ion possesses a large size, variable coordination numbers (from 6 to 8), and strong oxophilic properties which make it exhibit a high chemical activity to simultaneously combine inorganic O-enriched trilacunary Keggin POM fragments and organic O-donor ligands.[57] (3) The mal molecule with a chiral carbon atom, one hydroxyl group, and two carboxyl groups was expected to act as a structure-stabilizing agent and a chirality-inducing resource to construct chiral TMSPs. Fortunately, we successfully obtained the four homochiral POMs $(NH_4)_4(TMA)_4[Zr_4(\mu_3\text{-}O)_2(\text{L-mal})_2(B\text{-}\alpha\text{-}HSiW_{10}O_{37})_2]\cdot 19H_2O$ (**1a**), $(NH_4)_4(TMA)_4[Zr_4(\mu_3\text{-}O)_2(\text{D-mal})_2(B\text{-}\alpha\text{-}HSiW_{10}O_{37})_2]\cdot 24H_2O$ (**1b**), $(NH_4)_4(TMA)_4[Zr_4(\mu_3\text{-}O)_2(\text{L-mal})_2(B\text{-}\alpha\text{-}PW_{10}O_{37})_2]\cdot 14H_2O$ (**2a**), and $(NH_4)_4(TMA)_4[Zr_4(\mu_3\text{-}O)_2(\text{D-mal})_2(B\text{-}\alpha\text{-}PW_{10}O_{37})_2]\cdot 11H_2O$ (**2b**) and the mesomeric POM $(NH_4)_3Na_2K_5[Zr_4(\mu_3O)_2(\text{L-mal})(\text{D-mal})(B\text{-}\alpha\text{-}SiW_{10}O_{37})_2]\cdot 28H_2O$ (**3**). **1a,b** and **2a,b** are enantiomers, respectively, which exhibit obvious circular dichroism (CD) optical activity. As far as we are aware, **1** and **2** represent the first examples of enantiomerically pure Zr^{IV}-substituted Keggin POMs. Furthermore, **1** and **2** exhibit second harmonic generation response 0.8 times that of KDP.

EXPERIMENTAL SECTION

Materials and Methods. All reagents were acquired commercially and used without further purification. The lacunary precursors of $Na_{10}[A\text{-}\alpha\text{-}SiW_9O_{34}]\cdot 19H_2O$ and $Na_9[A\text{-}\alpha\text{-}PW_9O_{34}]\cdot 7H_2O$ were obtained according to previous literature methods.[58] FT-IR spectra were measured by using a Smart Omni-Transmission spectrometer in the 400−4000 cm^{-1} region with KBr pallets. The diffuse reflectance spectra were recorded on a PerkinElmer Lambda 900 UV/vis spectrophotometer equipped with an integrating sphere attachment and $BaSO_4$ as reference. Elemental analyses (C, H, N) were performed with a EuroEA 3000 CHNS/O elemental analyzer. Thermogravimetric analyses were carried out with a Mettler Toledo TGA/DSC 1000 analyzer under a dynamic air atmosphere with a heating rate of 20 °C min^{-1} in the temperature region of 30−1000 °C. Powder X-ray diffraction (PXRD) patterns were obtained on a Bruker D8 Advance XRD diffractometer with Cu Kα radiation (λ = 1.54056 Å) in the 2θ range of 5−55° at 293 K. Circular dichroism (CD) spectra in aqueous solution were collected by a Chirascan plus spectrometer at room temperature with a 0.1 mm path length cell under the following conditions: step size, 1 nm; bandwidth, 1.2 nm; time per point, 0.5 s. The second harmonic generation (SHG) signals were recorded on a Q-switched Nd:YAG solid-state laser with a wavelength of 1064 nm as the fundamental frequency using crystalline samples (70−100 mesh).

Syntheses of 1a,b. A mixture of $Na_{10}[A\text{-}\alpha\text{-}SiW_9O_{34}]\cdot 19H_2O$ (1.01 g, 0.36 mmol), $ZrOCl_2\cdot 8H_2O$ (0.24 g, 0.71 mmol), tetramethylammonium bromide (0.3 g, 1.95 mmol), NaCl (0.51 g, 8.71 mmol), NH_4Cl (0.31 g, 5.77 mmol), and L-/D-malic acid (0.27 g, 2.01 mmol; L-malic acid for **1a** and D-malic acid for **1b**) were added with stirring to a HOAc/NaOAc (0.5 M) buffer solution (pH 4.8, 5 mL). Then Na_2CO_3 (0.25 g, 2.36 mmol) was slowly added with continuous stirring for 30 min. The resulting emulsion was sealed in a 25 mL stainless steel reactor with a Teflon liner and heated at 120 °C for 5 days. After the mixture was cooled to room temperature, colorless block crystals were obtained. Yield: ca. 43% for **1a**, 45% for **1b** (based on $ZrOCl_2\cdot 8H_2O$). Anal. Calcd (found) for $C_{24}H_{114}O_{105}N_8Si_2Zr_4W_{20}$ (**1a**): C, 4.58 (4.69); H, 1.83 (1.97); N, 1.78 (1.70); Si, 0.89 (0.71); W, 58.43 (58.61); Zr, 5.80 (5.58). Calcd (found) for $C_{24}H_{124}O_{110}N_8Si_2Zr_4W_{20}$ (**1b**): C, 4.52 (4.65); H, 1.96 (2.10); N, 1.76 (1.67); Si, 0.88 (0.72); W, 57.60 (57.81); Zr, 5.72 (5.56).

Syntheses of 2a,b. **2a,b** were obtained by a procedure similar to that for **1a** and **1b**, except that $Na_{10}[A\text{-}\alpha\text{-}SiW_9O_{34}]\cdot 19H_2O$ and NaCl were replaced by $Na_9[A\text{-}\alpha\text{-}PW_9O_{34}]\cdot 7H_2O$ (1. 05 g, 0.41 mmol) and KCl (0.53 g, 7.07 mmol), respectively. Colorless strip crystals were acquired. Yield: ca. 37% for **2a**, 34% for **2b** (based on $ZrOCl_2\cdot 8H_2O$). Anal. Calcd (found) for $C_{24}H_{102}O_{100}\text{-}N_8P_2Zr_4W_{20}$ (**2a**): C, 4.64 (4.78); H, 1.66 (1.78); N, 1.81 (1.73); P, 1.00 (1.18); W, 59.24 (59.01); Zr, 5.88 (6.02). Calcd (found) for $C_{24}H_{96}O_{97}N_8P_2Zr_4W_{20}$ (**2b**): C, 4.69 (4.85); H, 1.57 (1.67); N, 1.82 (1.71); P, 1.01 (1.15); W, 59.76 (59.50); Zr, 5.93 (6.07).

Synthesis of 3. The preparation of **3** was identical to that of **1a** with mixed D-/L-malic acid (0.27 g, 2.01 mmol) in place of simplex L-malic acid. Colorless block crystals of **3** were obtained (29% yield based on $ZrOCl_2\cdot 8H_2O$). Anal. Calcd (found) for $C_8H_{78}O_{114}N_3Na_2K_5Si_2Zr_4W_{20}$ (**3**): C, 1.51 (1.65); H, 1.23 (1.41); N, 0.66 (0.79); Na, 0.72 (0.89); K, 3.06 (3.18); Si, 0.88 (0.76); W, 57.63 (57.39); Zr, 5.72 (5.88).

X-ray Structure Determination. The intensity data of **1−3** were collected on a Gemini A Ultra diffractometer equipped with graphite-monochromated Mo Kα (λ = 0.71073 Å) at room temperature. The SADABS program was used for the absorption correction. These structures were solved by direct methods and refined on F^2 by full-matrix least-squares methods using the SHELXTL-97 program package.[59,60] No hydrogen atoms associated with water molecules were located from the difference Fourier map. All hydrogen atoms attached to carbon atoms were geometrically placed and refined isotropically as a riding mode. In the structural refinements, the SQUEEZE function of PLATON was used to eliminate the residual electron density in the difference Fourier map which could not sensibly be assigned as disordered water molecules or cations (TMA cations and ammonium cations). The "ISOR" instruction was used for partial atoms to avoid NPD (nonpositive definite) and ADP (atomic displacement parameters) problems. The chemical structures of TMA cations and mal ligands were restrained with the commands "SIMU" and "DFIX". In **1a,b** and **2a,b**, three TMA and partial ammonium cations and lattice water molecules can be assigned from residual peaks. The final molecular formulas of **1−3** were defined by a combination of the results of elemental analysis, IR (Figure S1), TGA (Figure S2), and charge balance considerations. Crystallographic data and structure refinement information for **1−3** are outlined in Table 1. CCDC 1875066 (**1a**), 1875067 (**1b**), 1875069 (**2a**), 1875070 (**2b**),

DOI: 10.1021/acs.inorgchem.9b00258
Inorg. Chem. 2019, 58, 4657−4664

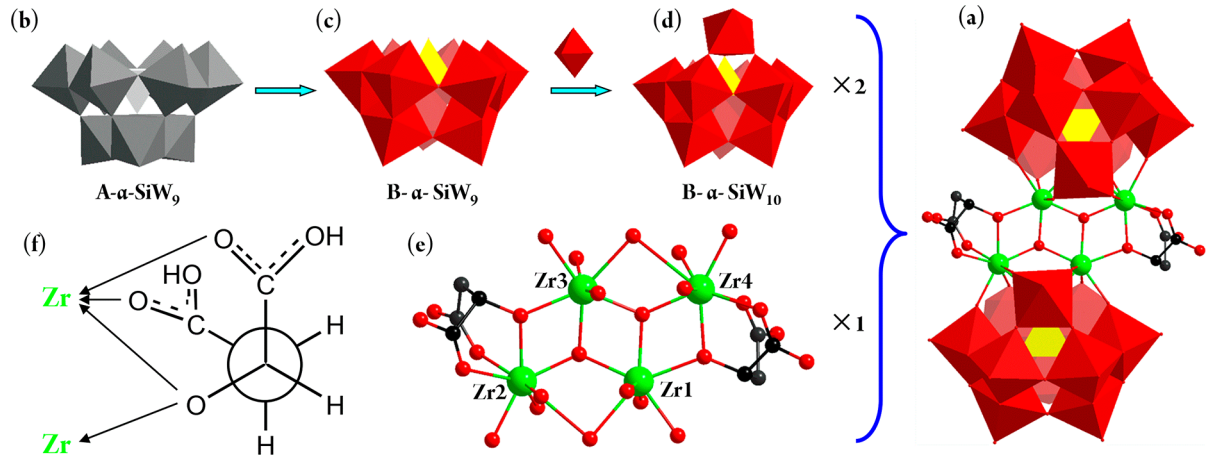

Figure 1. (a) Polyhedral/ball-and-stick representation of tetra-Zr^{IV}-substituted sandwich-type $[Zr_4(\mu_3\text{-}O)_2(\text{L-mal})_2(\text{B-}\alpha\text{-}SiW_{10}O_{37})_2]^{10-}$ polyoxoanion. (b–d) Schematic transformation from $[\text{A-}\alpha\text{-}SiW_9O_{34}]^{10-}$ to $[\text{B-}\alpha\text{-}SiW_{10}O_{37}]^{10-}$ via $[\text{B-}\alpha\text{-}SiW_9O_{34}]^{10-}$. (e) Ball-and-stick representation of $\{Zr_4\}$ cluster. (f) Newman projection and coordination environment of the L-mal ligand. Color codes: O, red; C, black; Si, yellow; Zr, green. Hydrogen atoms are omitted for clarity.

and 1875068 (**3**) contain supplementary crystallographic data for this paper.

RESULTS AND DISCUSSION

Crystal Structures of 1 and 2. The experimental PXRD peaks of the five compounds are in accordance with the simulated XRD peaks, indicating good purity of the sample phases (Figure S3). Single-crystal X-ray diffraction shows that **1a,b** and **2a,b** are isostructural. Therefore, we describe the crystal structures of **1a,b** in detail as examples. **1a,b** crystallize in the chiral orthorhombic space group $P2_12_12_1$ with near-zero Flack parameters of −0.008(7) for **1a** and −0.021(8) for **1b**, corroborating the absolute configuration in the crystals.[61] The molecular structure of **1a** consists of the tetra-Zr^{IV}-substituted sandwich-type polyoxoanion $[Zr_4(\mu_3\text{-}O)_2(\text{L-mal})_2(\text{B-}\alpha\text{-}SiW_{10}O_{37})_2]^{10-}$ (Figure 1a), 4 TMA cations, 4 ammonium cations, 2 protons, and 19 lattice water molecules. In the tetra-Zr^{IV}-substituted sandwich-type polyoxoanion of **1a**, four crystallographically independent Zr^{4+} ions occupy the vacant positions of in situ generated Keggin $[\text{B-}\alpha\text{-}SiW_{10}O_{37}]^{10-}$ moieties (Figure 1d) from the precursor[62,63] (Figure 1b) and form a rhombic $\{Zr_4(\mu_3\text{-}O)_2(\text{L-mal})_2\}\{Zr_4\}$ cluster (Figure 1e) through two μ_3-O atoms, which is decorated by two of the same chiral L-mal ligands (Figure 1f and Figure S4) with a μ_2-η^1:η^2:η^1 bridging mode on each side of the sandwich-type polyoxoanion. In the $\{Zr_4\}$ cluster, the Zr^{4+} ions can be divided into two types on the basis of coordination modes: $Zr1^{4+}$ and $Zr3^{4+}$ ions are heptacoordinated by four O atoms from one Keggin $[\text{B-}\alpha\text{-}SiW_{10}O_{37}]^{10-}$ fragment, two μ_3-O bridges, and one O atom from the hydroxyl group of a L-mal ligand, which exhibit a distorted-pentagonal-bipyramidal geometry (Figure S5); $Zr2^{4+}$ and $Zr4^{4+}$ ions are octacoordinated by four O atoms from one Keggin $[\text{B-}\alpha\text{-}SiW_{10}O_{37}]^{10-}$ fragment, one μ_3-O bridge, two O atoms from the carboxyl group of a L-mal ligand, and one O atom from the hydroxyl group of an L-mal ligand, which show a decahedral geometry (Figure S5). Bond-valence-sum (BVS) calculations indicate that the oxidation states of all W and Zr centers are +6 and +4, respectively, and the terminal O atoms (O80, O81, O84, and O85) of carboxyl in L-mal are protonated (Table S1). The Zr−O_{mal} bond lengths vary form 2.149(17) to 2.305(19) Å (Table S2). These structural parameters are analogous to those of **1b** (Figure S6) except that 2 of the same chiral D-mal ligands were employed and 24 lattice water molecules were found in the latter.

Helical structures are closely related to chirality and have been attracting increased attention in coordination chemistry and materials chemistry. Interestingly, the structures of **1a,b** exhibit unique 1D right- and left-handed helical chains with a 2_1 screw axis (Figure 2), respectively, which are constructed

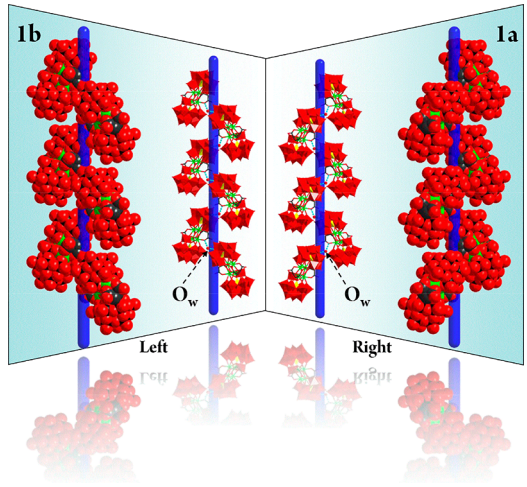

Figure 2. Right- and left-handed helical chains constructed from adjacent sandwich-type polyoxoanions via hydrogen-bonding interactions in **1a,b**. Hydrogen and NH_4^+ and TMA ions are omitted for charity.

from adjacent sandwich-type polyoxoanions via hydrogen-bonding interactions between O1W atoms and surface O atoms from sandwich-type polyoxoanions (Table S3). These inorganic−organic hybrid helical chains in **1a,b** are mirror symmetrical. The initial chiral mal ligands may be expected to be responsible for the formation of the helical chains in **1a,b**.

Crystal Structure of 3. Single-crystal X-ray diffraction reveals that **3** crystallizes in the monoclinic space group *C*2/*c*. The molecular structure of **3** contains the tetra-Zr^{IV} substituted sandwich-type polyoxoanion $[Zr_4(\mu_3\text{-}O)_2(\text{L-mal})(\text{D-mal})(\text{B-}\alpha\text{-}SiW_{10}O_{37})_2]^{10-}$ (Figure 3b and Figure S7), 2 Na^+ ions, 5 K^+ ions, 3 ammonium cations, and 28 lattice water molecules.

DOI: 10.1021/acs.inorgchem.9b00258
Inorg. Chem. 2019, 58, 4657−4664

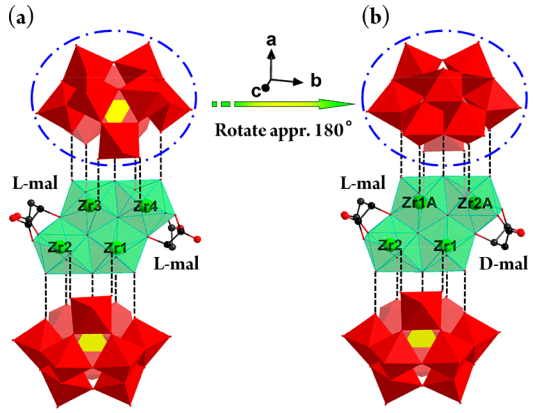

Figure 3. Comparison of tetra-Zr^{IV}-substituted sandwich-type polyoxoanions in **1a** (a) and **3** (b). The hydrogen atoms attached to carbon atoms are omitted for charity.

Different from the case for **1** and **2**, a pair of opposite chiral L- and D-mal ligands is simultaneously installed to the central rhombic $\{Zr_4\}$ cluster in **3**, which endows the tetra-Zr^{IV}-substituted sandwich-type polyoxoanion with centrosymmetry. As a result, there are two independent Zr^{4+} ions in the $\{Zr_4\}$ cluster: the $Zr1^{4+}$ ion utilizes a heptacoordinate mode while the $Zr2^{4+}$ ion exhibits an octacoordinate mode (Table S5). Intuitively, the configuration of the tetra-Zr^{IV}-substituted sandwich-type polyoxoanion in **3** can be regarded as the result of upper lacunary units $[B\text{-}\alpha\text{-}SiW_{10}O_{37}]^{10-}$ in **1a** rotating approximate 180° along the *a* axis, demonstrating that the chirality of mal ligands significantly affects the structure of POM clusters (Figure 3). In addition, **3** is virtually similar to the centrosymmetric complex $[Zr_4(\mu_3\text{-}O)_2(\mu\text{-}O)_2(L)_2(B\text{-}\alpha\text{-}XW_{10}O_{37})_2]$ (X = Si^{IV}, Ge^{IV}; L = oxalate/tris(hydroxymethyl)-aminomethane,[62,63] acetate,[64] H_2O,[65] and mandelic[57]) previously reported by Yang and Kortz et al.

The most striking structural feature of **3** is that each $[Zr_4(\mu_3\text{-}O)_2$(L-mal)(D-mal)$(B\text{-}\alpha\text{-}SiW_{10}O_{37})_2]^{10-}$ polyoxoanion joins adjacent six $K2^+$ bridges and each $K2^+$ bridge links to adjacent three $[Zr_4(\mu_3\text{-}O)_2$(L-mal)(D-mal)$(B\text{-}\alpha\text{-}SiW_{10}O_{37})_2]^{10-}$ polyoxoanions, leading to a 2D layer (Figure 4a). Furthermore, adjacent 2D layers are interconnected by two $Na1^+$ cations along the *c* axis (Figure 4b), forming a 3D (3,10)-connected framework with a Schläfli symbol of $\{4^{18}.6^{24}.8^3\}\text{-}\{4^3\}_2$ (Figure 5).

CD Spectra. In order to verify the chiral optical activities of enantiomers, the CD spectra of **1a**,**b** and **2a**,**b** in aqueous solution were measured. As shown in Figure 6, the CD spectra for **1a**,**b** are mirror symmetrical and display strong Cotton effects with four bands at 221, 230, 254, and 279 nm ($\Delta\varepsilon_{max} \approx 3.7/-3.7$ $M^{-1}cm^{-1}$ for **1a**/**1b**), indicating that **1a**,**b** are enantiomers.[66,2] The CD spectra of **1a**,**b** are observably different from the chirality-inducing agents L-mal and D-mal (Figure 6 insert), which only show a weak Cotton effect with a band ($\Delta\varepsilon_{max}$ less than 1 M^{-1} cm^{-1}) at 218 nm and are almost CD silent above 250 nm. In contrast, **1a**,**b** exhibit strong Cotton effects up to 300 nm, which are derived from the oxygen to tungsten charge-transfer transitions of polyoxoanions.[67] These results adequately demonstrate that the induced CD phenomenon in **1a**,**b** results from the chirality transfer from the small chiral L-mal or D-mal ligands to the large substituted metal−oxygen clusters. The intensities of CD spectra for **1a**,**b** are stronger than those of previously reported

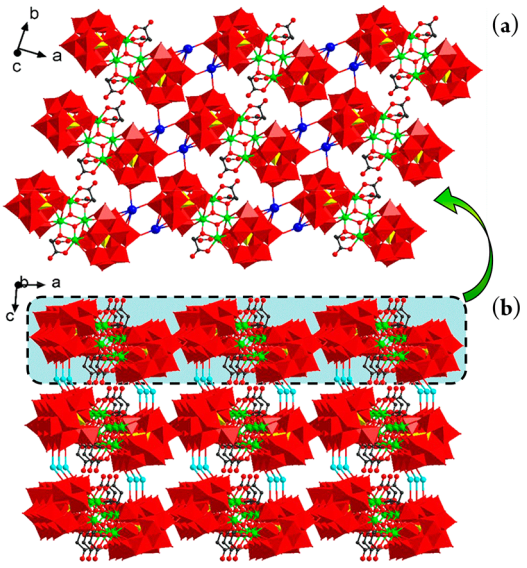

Figure 4. (a) The 2D layer of **3** formed by $[Zr_4(\mu_3\text{-}O)_2$(L-mal)(D-mal)$(B\text{-}\alpha\text{-}SiW_{10}O_{37})_2]^{10-}$ units and K_2^+ bridges. (b) The 3D network of **3** constructed from 2D layers linked by Na_1^+ ions. Color codes: WO_6 octahedra, red; SiO_4 tetrahedra, yellow; $K2^+$ ions, blue; $Na1^+$ ions, sky blue.

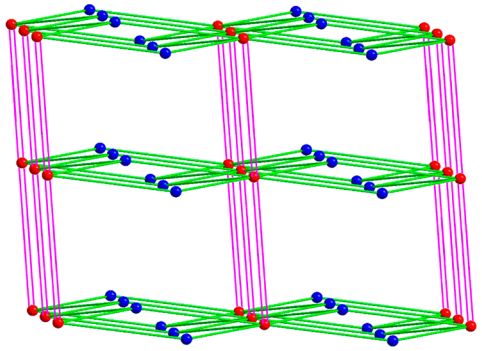

Figure 5. Topological view of the 3D (3,10)-framework in **3**. Color code: red balls, $[Zr_4(\mu_3\text{-}O)_2$(L-mal)(D-mal)$(B\text{-}\alpha\text{-}SiW_{10}O_{37})_2]^{10-}$ nodes; blue balls, $K2^+$ bridges; pink rods, $Na1^+$ linkers.

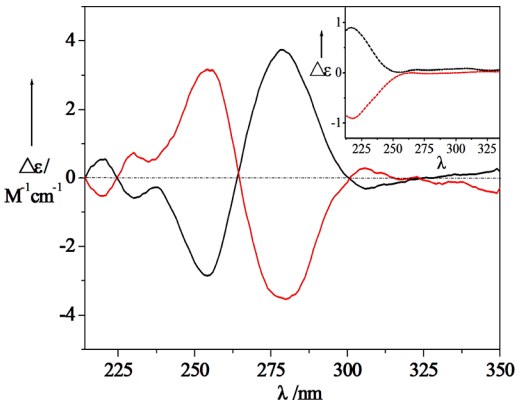

Figure 6. CD spectra of **1a** (black solid line, $c = 4.29 \times 10^{-5}$ M), **1b** (red solid line, $c = 4.23 \times 10^{-5}$ M), L-malic acid (inset, black dashed line), and D-malic acid (inset, red dashed line) in aqueous solution.

Dawson-type chiral POMs ($\Delta\varepsilon \approx 2.3$ M^{-1} cm^{-1}).[43] The CD spectra of **2a**,**b** in aqueous solution are shown in Figure S8, which reveal Cotton effects similar to those of **1a**,**b**. In

DOI: 10.1021/acs.inorgchem.9b00258
Inorg. Chem. 2019, 58, 4657−4664

addition, the UV−vis spectra of **1a**,**b** and **2a**,**b** are virtually unchanged with time, indicating that the two pairs of enantiomers are stable in water solution (Figure S9).[2,45]

Optical Band Gaps. To evaluate the optical semiconductor behaviors of **1**−**3**, the diffuse reflectance spectra for their crystalline samples were obtained at room temperature to obtain their optical band gaps (E_g). The optical band gaps of **1**−**3** were determined as cross points between the E_g axis and the line extrapolated from the linear portion of the absorption edge in the curve of the Kubelka−Munk (K-M) function versus energy.[68,69] As shown in Figure S10, the band gaps of **1a**,**b**, **2a**,**b**, and **3** are 3.53, 3.55, 3.57, 3.56, and 3.54 eV, respectively, indicating that they are potential optical semiconductor materials and may have the capacity for photocatalytic reactions.

SHG Response. Nonlinear optical (NLO) materials have attracted great interest for their wide range of applications in laser technology, data storage, telecommunications, and optical switches.[70] **1a**,**b** and **2a**,**b** crystallize in the chiral space group $P2_12_12_1$, which prompted us to investigate their NLO properties. The SHG signals of **1a** and **2a** as examples were measured on a Q-switched Nd:YAG laser. The results indicate that **1a** and **2a** display obvious SHG response and their response intensities are approximately 0.8 times that of KDP (KH_2PO_4) (Figure 7 and Figure S11).

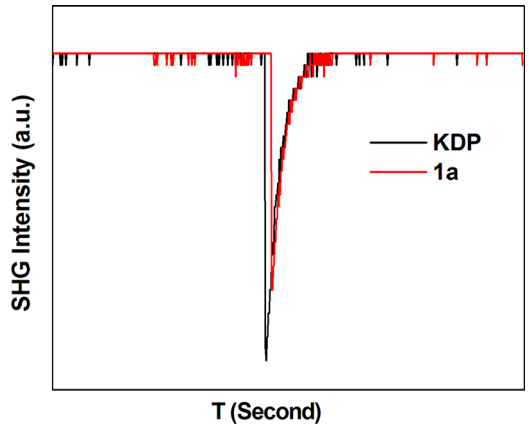

Figure 7. Oscilloscope traces of SHG signals for **1a** and KDP at the same particle size of 70−100 mesh.

CONCLUSIONS

In summary, we synthesized two pairs of enantiomeric malate chirality-inducing tetra-Zr^{IV}-substituted POMs **1a**/**1b** and **2a**/**2b** and the mesomeric tetra-Zr^{IV}-substituted POM **3** under hydrothermal conditions. The CD spectra of **1** and **2** show strong Cotton effects, proving that the induced CD phenomenon in **1** and **2** results from the chirality transfer from the small chiral L-mal or D-mal ligands to the large substituted metal−oxygen clusters. UV−vis diffuse reflectance spectra reveal that **1**−**3** are potential optical semiconductor materials. Moreover, **1a** and **2a** exhibit an obvious SHG response. **1** and **2** represent the first examples of enantiomerically pure Zr^{IV}-substituted Keggin POMs. Their successful syntheses not only reveal the relationship of structure and optical activity at the molecular level but also confirm the rational design synthetic strategy of using the synergistic effect of lacunary POM structure-directing function and chiral ligand inducting role to construct functional Keggin TMSP-based materials by hydrothermal technology.

ASSOCIATED CONTENT

Supporting Information

The Supporting Information is available free of charge on the ACS Publications website at DOI: 10.1021/acs.inorgchem.9b00258.

Selected bond distances, PXRD patterns, IR and UV−vis diffuse reflectance spectra, TGA of **1**−**3**, liquid-state CD spectra of **2**, and additional structures (PDF)

Accession Codes

CCDC 1875066−1875070 contain the supplementary crystallographic data for this paper. These data can be obtained free of charge via www.ccdc.cam.ac.uk/data_request/cif, or by emailing data_request@ccdc.cam.ac.uk, or by contacting The Cambridge Crystallographic Data Centre, 12 Union Road, Cambridge CB2 1EZ, UK; fax: +44 1223 336033.

AUTHOR INFORMATION

Corresponding Authors

*E-mail for J.-W.Z.: zhaojunwei@henu.edu.cn.
*E-mail for G.-Y.Y.: ygy@bit.edu.cn.

ORCID

Jun-Wei Zhao: 0000-0002-7685-1309
Guo-Yu Yang: 0000-0002-0911-2805

Notes

The authors declare no competing financial interest.

ACKNOWLEDGMENTS

This work was supported by the National Natural Science Foundation of China (nos. 21571016, 21831001, 91122028, 21571048, 21771052) and the National Natural Science Foundation of China for Distinguished Young Scholars (no. 20725101).

REFERENCES

(1) Crassous, J. Chiral transfer in coordination complexes: towards molecular materials. *Chem. Soc. Rev.* **2009**, *38*, 830−845.
(2) An, H. Y.; Wang, E. B.; Xiao, D. R.; Li, Y. G.; Su, Z. M.; Xu, L. Chiral 3D architectures with helical channels constructed from polyoxometalate clusters and copper-amino acid complexes. *Angew. Chem., Int. Ed.* **2006**, *45*, 904−908.
(3) Prins, L. J.; Huskens, J.; Jong, F. D.; Timmerman, P.; Reinhoudt, D. N. Complete asymmetric induction of supramolecular chirality in a hydrogen-bonded assembly. *Nature* **1999**, *398*, 498−502.
(4) Soghomonian, V.; Chen, Q.; Haushalter, R. C.; Zubieta, J.; O'Connor, C. J. An inorganic double helix: hydrothermal synthesis, structure, and magnetism of chiral $[(CH_3)_2NH_2]K_4[V_{10}O_{10}(H_2O)_2(OH)_4(PO_4)_7]\cdot 4H_2O$. *Science* **1993**, *259*, 1596−1599.
(5) Yang, X. J.; Bao, S. S.; Zheng, T.; Zheng, L. M. An enantioenriched vanadium phosphonate generated via asymmetric chiral amplification of crystallization from achiral sources showing a single-crystal-to-single-crystal dehydration process. *Chem. Commun.* **2012**, *48*, 6565−6567.
(6) Liu, Y.; Xuan, W.; Cui, Y. Engineering homochiral metal-organic frameworks for heterogeneous asymmetric catalysis and enantioselective separation. *Adv. Mater.* **2010**, *22*, 4112−4135.
(7) Song, C. E.; Lee, S. G. Supported chiral catalysts on inorganic materials. *Chem. Rev.* **2002**, *102*, 3495−3525.
(8) Ngo, H. L.; Lin, W. Hybrid organic-inorganic solids for heterogeneous asymmetric catalysis. *Top. Catal.* **2005**, *34*, 85−92.

DOI: 10.1021/acs.inorgchem.9b00258
Inorg. Chem. 2019, 58, 4657−4664

(9) Ma, L.; Abney, C.; Lin, W. Enantioselective catalysis with homochiral metal-organic frameworks. *Chem. Soc. Rev.* **2009**, *38*, 1248−1256.
(10) Seo, J. S.; Whang, D.; Lee, H.; Jun, S. I.; Oh, J.; Jeon, Y. J.; Kim, K. A homochiral metal-organic porous material for enantioselective separation and catalysis. *Nature* **2000**, *404*, 982−986.
(11) Fang, W. H.; Zhang, L.; Zhang, J.; Yang, G. Y. Water-stable homochiral cluster organic frameworks built by two kinds of large tetrahedral cluster units. *Chem. - Eur. J.* **2016**, *22*, 2611−2615.
(12) Cao, G. J.; Fang, W. H.; Zheng, S. T.; Yang, G. Y. $(CH_3NH_3)_2[Ge(B_4O_9)]$: an organically-templated chiral borogermanate with second-order nonlinear and ferroelectric properties. *Inorg. Chem. Commun.* **2010**, *13*, 1047−1049.
(13) Lacroix, P. G. Second-order optical nonlinearities in coordination chemistry: the case of bis(salicylaldiminato)metal schiff base complexes. *Eur. J. Inorg. Chem.* **2001**, *2001*, 339−348.
(14) Barron, L. D. Chirality and life. *Space Sci. Rev.* **2008**, *135*, 187−201.
(15) Wang, Y.; Huang, H.; Zhang, Q.; Zhang, P. Chirality in metal-based anticancer agents. *Dalton Trans.* **2018**, *47*, 4017−4026.
(16) Hill, C. L. Introduction: polyoxometalates multicomponent molecular vehicles to probe fundamental issues and practical problems. *Chem. Rev.* **1998**, *98*, 1−2.
(17) Dolbecq, A.; Dumas, E.; Mayer, C. R.; Mialane, P. Hybrid organic-inorganic polyoxometalate compounds: from structural diversity to applications. *Chem. Rev.* **2010**, *110*, 6009−6048.
(18) Zhao, J. W.; Li, B.; Zheng, S. T.; Yang, G. Y. Two-dimensional extended (4,4)-topological network constructed from tetra-Ni^{II}-substituted sandwich-type Keggin polyoxometalate building blocks and Ni^{II}-organic cation bridges. *Cryst. Growth Des.* **2007**, *7*, 2658−2664.
(19) Liu, J. C.; Han, Q.; Chen, L. J.; Zhao, J. W.; Streb, C.; Song, Y. F. Aggregation of giant cerium-bismuth tungstate clusters into a 3D porous framework with high proton conductivity. *Angew. Chem., Int. Ed.* **2018**, *57*, 8416−8420.
(20) Gu, Y. N.; Chen, Y.; Wu, Y. L.; Zheng, S. T.; Li, X. X. A series of banana-shaped 3d-4f heterometallic cluster substituted polyoxometalates: syntheses, crystal structures, and magnetic properties. *Inorg. Chem.* **2018**, *57*, 2472−2479.
(21) Huang, L.; Wang, S. S.; Zhao, J. W.; Cheng, L.; Yang, G. Y. Synergistic combination of multi-Zr^{IV} cations and lacunary Keggin germanotungstates leading to a gigantic Zr_{24}-cluster-substituted polyoxometalate. *J. Am. Chem. Soc.* **2014**, *136*, 7637−7642.
(22) Lv, H.; Guo, W.; Wu, K.; Chen, Z.; Bacsa, J.; Musaev, D. G.; Geletii, Y. V.; Lauinger, S. M.; Lian, T.; Hill, C. L. A noble-metal-free, tetra-nickel polyoxotungstate catalyst for efficient photocatalytic hydrogen evolution. *J. Am. Chem. Soc.* **2014**, *136*, 14015−14018.
(23) Hasenknopf, B. Polyoxometalates: introduction to a class of inorganic compounds and their biomedical applications. *Front. Biosci., Landmark Ed.* **2005**, *10*, 275−287.
(24) Bijelic, A.; Rompel, A. Ten good reasons for the use of the tellurium-centered Anderson-Evans polyoxotungstate in protein crystallography. *Acc. Chem. Res.* **2017**, *50*, 1441−1448.
(25) Bijelic, A.; Rompel, A. The use of polyoxometalates in protein crystallography − an attempt to widen a well-known bottleneck. *Coord. Chem. Rev.* **2015**, *299*, 22−38.
(26) Rhule, J. T.; Hill, C. L.; Judd, D. A. Polyoxometalates in medicine. *Chem. Rev.* **1998**, *98*, 327−358.
(27) Bijelic, A.; Aureliano, M.; Rompel, A. Polyoxometalates as potential next-generation metallodrugs in the combat against cancer. *Angew. Chem., Int. Ed.* **2019**, *58*, 2980−2999.
(28) Bijelic, A.; Aureliano, M.; Rompel, A. The antibacterial activity of polyoxometalates: structures, antibiotic effects and future perspectives. *Chem. Commun.* **2018**, *54*, 1153−1169.
(29) Nisar, A.; Lu, Y.; Zhuang, J.; Wang, X. Polyoxometalate nanocone nanoreactors: magnetic manipulation and enhanced catalytic performance. *Angew. Chem., Int. Ed.* **2011**, *50*, 3187−3192.
(30) Paille, G.; Gomez-Mingot, M.; Roch-Marchal, C.; Lassalle-Kaiser, B.; Mialane, P.; Fontecave, M.; Mellot-Draznieks, C.; Dolvecq, A. A fully noble metal-free photosystem based on cobalt-polyoxometalates immobilized in a porphyrinic metal-organic framework for water oxidation. *J. Am. Chem. Soc.* **2018**, *140*, 3613−3618.
(31) Xue, H.; Zhang, Z.; Pan, R.; Yang, B. F.; Liu, H. S.; Yang, G. Y. Supramolecular nanotubes constructed from 3d-4f hetero-metallic sandwiched polyoxotungstate dimers. *CrystEngComm* **2016**, *18*, 4643−4650.
(32) Han, Q.; Liu, J. C.; Wen, Y.; Chen, L. J.; Zhao, J. W.; Yang, G. Y. Tellurotungstate-based organotin−rare-earth heterometallic hybrids with four organic components. *Inorg. Chem.* **2017**, *56*, 7257−7269.
(33) Zhang, Z. M.; Duan, X.; Yao, S.; Wang, Z.; Lin, Z.; Li, Y. G.; Long, L. S.; Wang, E. B.; Lin, W. Cation-mediated optical resolution and anticancer activity of chiral polyoxometalates built from entirely achiral building blocks. *Chem. Sci.* **2016**, *7*, 4220−4229.
(34) Du, D. Y.; Yan, L. K.; Su, Z. M.; Li, S. L.; Lan, Y. Q.; Wang, E. B. Chiral polyoxometalate-based material: from design syntheses to functional applications. *Coord. Chem. Rev.* **2013**, *257*, 702−717.
(35) Haasenknopf, B.; Micoine, K.; Lacôte, E.; Thorimbert, S.; Malacria, M.; Thouvenot, R. Chirality in polyoxometalate chemistry. *Eur. J. Inorg. Chem.* **2008**, *2008*, 5001−5013.
(36) Carraro, M.; Sartorel, A.; Scorrano, G.; Maccato, C.; Dickman, M. H.; Kortz, U.; bonchio, M. Chiral Strandberg-type molybdates $[(RPO_3)_2Mo_2O_{15}]^{2-}$ as molecular gelators: self-assembled fibrillar nanostructures with enhanced optical activity. *Angew. Chem., Int. Ed.* **2008**, *47*, 7275−7279.
(37) Micoine, K.; Hasenknopf, B.; Thorimbert, S.; Lacôte, E.; Malacria, M. Chiral recognition of hybrid metal oxide by peptides. *Angew. Chem., Int. Ed.* **2009**, *48*, 3466−3468.
(38) Han, Q.; He, C.; Zhao, M.; Qi, B.; Niu, J.; Duan, C. Engineering chiral polyoxometalate hybric metal-organic frameworks for asymmetric dihydroxylation of olefins. *J. Am. Chem. Soc.* **2013**, *135*, 10186−10189.
(39) Xiao, F.; Hao, J.; Lv, C.; Yin, P.; Wang, L.; Wei, Y. Polyoxometalatocyclophanes: controlled assembly of polyoxometalate-based chiral metallamacrocycles from achiral building blocks. *J. Am. Chem. Soc.* **2010**, *132*, 5956−5957.
(40) Kapakoglou, N. L.; Panagiotis, B. L.; Kazianis, S. E.; Kosmidis, C. E.; Drouza, C.; Manos, M. J.; Sigalas, M. P.; Keramidas, A. D.; Kabanos, T. A. Polyoxomolybdenum(V/VI)-sulfite compounds: synthesis, structural, and physical studies. *Inorg. Chem.* **2007**, *46*, 6002−6010.
(41) Li, H. L.; Liu, Y. J.; Liu, J. L.; Chen, L. J.; Zhao, J. W.; Yang, G. Y. Structural transformation from dimerization to tetramerization of serine-decorated rare-earth incorporated arsenotungstates induced by the usage of rare-earth salts. *Chem. - Eur. J.* **2017**, *23*, 2673−2689.
(42) Fang, X.; Anderson, T. M.; Hill, C. L. Enantiomerically pure polytungstates: chirality transfer through zirconium coordination centers to nanosized inorganic clusters. *Angew. Chem., Int. Ed.* **2005**, *44*, 3540−3544.
(43) Fang, X.; Anderson, T. M.; Hou, Y.; Hill, C. L. Stereoisomerism in polyoxometalates: structural and spectroscopic studies of bis-(malate) functionalized cluster systems. *Chem. Commun.* **2005**, *40*, 5044−5046.
(44) Knoth, W. H.; Harlow, R. L. New tungstophosphates: $Cs_6W_5P_2Na_2W_{10}PO_{37}$. *J. Am. Chem. Soc.* **1981**, *103*, 1865−1867.
(45) Tang, Q.; Liu, S.; Liu, Y.; Li, S.; Ma, F.; Li, J.; Wang, S.; Liu, C. Assembly and spontaneous resolution of the chiral inorganic polyoxometalates-based frameworks via helical chains association. *Dalton Trans.* **2013**, *42*, 8512−8518.
(46) Zheng, S. T.; Zhang, J.; Yang, G. Y. Designed synthesis of POM-organic frameworks from $\{Ni_6PW_9\}$ building blocks under hydrothermal conditions. *Angew. Chem., Int. Ed.* **2008**, *47*, 3909−3913.
(47) Wang, Y.; Li, H.; Qi, W.; Yang, Y.; Yan, Y.; Li, B.; Wu, L. Supramolecular assembly of chiral polyoxometalate complexes for asymmetric catalytic oxidation of thioethers. *J. Mater. Chem.* **2012**, *22*, 9181−9188.

DOI: 10.1021/acs.inorgchem.9b00258
Inorg. Chem. 2019, 58, 4657−4664

(48) Attoui, M.; Pouget, E.; Oda, R.; Talaga, D.; Bourdon, G. L.; Buffeteau, T.; Nlate, S. Optically active polyoxometalate-based silica nanohelices: induced chirality from inorganic nanohelices to achiral POM clusters. *Chem. - Eur. J.* **2018**, *24*, 11344−11353.
(49) Lu, M.; Kang, J.; Wang, D.; Peng, Z. Enantiopure 1,1′-binaphthly-based polyoxometalate-containing molecular hybrids. *Inorg. Chem.* **2005**, *44*, 7711−7713.
(50) Carraro, M.; Modugno, G.; Sartorel, A.; Scorrano, G.; Bonchio, M. Optically active polyoxotungstates bearing chiral oganophosphonate substituents. *Eur. J. Inorg. Chem.* **2009**, *2009*, 5164−5174.
(51) Ishimoto, R.; Kamata, K.; Suzuki, K.; Yamaguchi, K.; Mizuno, N. Synthesis and structural characterization of BINOL-modified chiral polyoxometalates. *Dalton Trans.* **2015**, *44*, 10947−10951.
(52) Zheng, S. T.; Zhang, J.; Clemente-Juan, J. M.; Yuan, D. Q.; Yang, G. Y. Poly(polyoxotungstate)s with 20 nickel centers: from nanoclusters to one-dimensional chains. *Angew. Chem., Int. Ed.* **2009**, *48*, 7176−7179.
(53) Zhao, J. W.; Wang, C. M.; Zhang, J.; Zheng, S. T.; Yang, G. Y. Combination of lacunary polyoxometalates and high-nuclear transition metal clusters under hydrothermal conditions: IX. A series of novel polyoxotungstates sandwiched by octa-copper clusters. *Chem. - Eur. J.* **2008**, *14*, 9223−9239.
(54) Xue, H.; Zhao, J. W.; Pan, R.; Yang, B. F.; Yang, G. Y.; Liu, H. S. Diverse ligand-functionalized mixed-valent hexa-manganese sandwiched silicotungstates with single-molecule magnet behavior. *Chem. - Eur. J.* **2016**, *22*, 12322−12331.
(55) Li, H. L.; Wang, Y. L.; Zhang, Z.; Yang, B. F.; Yang, G. Y. A new tetra-Zr(IV)-substituted poloxotungstate aggregate. *Dalton Trans.* **2018**, *47*, 14017−14027.
(56) Zheng, S. T.; Yang, G. Y. Recent advances in paramagnetic-TM-substituted polyoxometalstes (TM = Mn, Fe, Co Ni, Cu). *Chem. Soc. Rev.* **2012**, *41*, 7623−7646.
(57) Li, D.; Han, H.; Wang, Y.; Wang, X.; Li, Y.; Wang, E. Modification of tetranuclear zirconium-substituted polyoxometalates-syntheses, structures, and peroxidase-like catalytic activities. *Eur. J. Inorg. Chem.* **2013**, *2013*, 1926−1934.
(58) Ginsberg, A. P. *Inorg. Synth.* **1990**, *27*, 87−100.
(59) Sheldrick, G. M. *SHELXS 97, Program for crystal structure solution*; University of Göttingen: Göttingen, Germany, 1997.
(60) Sheldrick, G. M. *SHELXS 97, program for crystal structure refinement*; University of Göttingen: Göttingen, Germany, 1997.
(61) Flack, H. D. On enantiomorgh-polarity estimation. *Acta Crystallogr., Sect. A: Found. Crystallogr.* **1983**, *A39*, 876−881.
(62) Wang, Y. L.; Zhang, Z.; Li, H. L.; Li, X. Y.; Yang, G. Y. An oxalate-functionalized tetra-Zr^{IV}-substituted sandwich-type silicotungstate: hydrothermal synthesis, structural characterization, and catalytic oxidation of thioethers. *Eur. J. Inorg. Chem.* **2019**, *2019*, 417−422.
(63) Zhang, Z.; Wang, Y. L.; Yang, G. Y. Two inorganic-organic hybrid polyoxotungstates constructed from tetra-Zr^{IV}-substituted sandwich-type germanetungstates functionalized by tris ligand. *Inorg. Chem. Commun.* **2017**, *85*, 32−36.
(64) Chen, L.; Liu, Y.; Chen, S.; Hu, H.; Fu, F.; Wang, J.; Xue, G. Acetate-functionalized zirconium-substituted tungstogermanate, $[Zr_4O_2(OH)(CH_3COO)_2(\alpha\text{-}GeW_{10}O_{37})_2]^{12-}$. *J. Cluster Sci.* **2009**, *20*, 331−340.
(65) Bassil, B. S.; Dickman, M. H.; Kortz, U. Synthesis and structure of asymmetric zirconium-substituted silicotungstates, $[Zr_6O_2(OH)_4(H_2O)_3(\alpha\text{-}SiW_{10}O_{37})_3]^{14-}$ and $[Zr_4O_2(OH)_2(H_2O)_4(\beta\text{-}SiW_{10}O_{37})_2]^{10-}$. *Inorg. Chem.* **2006**, *45*, 2394−2396.
(66) Ju, W. W.; Zhang, H. T.; Xu, X.; Zhang, Y.; Xu, Y. Enantiomerically pure lanthanide-organic polytungstates exhibiting two-photon absorption properties. *Inorg. Chem.* **2014**, *53*, 3269−3271.
(67) Tézé, A.; Canny, J.; Gurban, L.; Thouvenot, R.; Hervé, G. Synthesis, structural characterization, and oxidation reduction behavior of the γ−isomer of the dodecatungsto-silicate anion. *Inorg. Chem.* **1996**, *35*, 1001−1005.
(68) Wesley, W. M.; Harry, W. G. H. *Reflectance Spectroscopy*; Wiley: New York, 1966.
(69) Pankove, J. I. *Optical Processes in Semiconductors*; Prentice-Hall: New York, 1997.
(70) Zhang, X. M.; Shan, B. Z.; Duan, C. Y.; You, X. Z. Second-order non-linear optical response of a novel type of charge-transfer complex $[4\text{-DMSP}]_4[NH_2Me_2]_2HSiFeMo_{11}O_{40}\cdot 3H_2O$. *Chem. Commun.* **1997**, *41*, 1131−1132.

NOTE ADDED AFTER ASAP PUBLICATION

This paper was published on the Web on March 18, 2019. Additional text corrections were added, and the corrected version was reposted on April 1, 2019.

DOI: 10.1021/acs.inorgchem.9b00258
Inorg. Chem. 2019, 58, 4657−4664